Available online at www.sciencedirect.com
SCIENCE DIRECT
Journal of Solid State Chemistry 179 (2006) 1345–1350
JOURNAL OF SOLID STATE CHEMISTRY
www.elsevier.com/locate/jssc

Synthesis, structure, and characterization of a new one-dimensional tellurite phosphate, $Ba_2TeO(PO_4)_2$

Kang Min Ok, P. Shiv Halasyamani*

Department of Chemistry and Center for Materials Chemistry, University of Houston, 136 Fleming Building, Houston, TX 77204-5003, USA

Received 9 December 2005; received in revised form 20 January 2006; accepted 22 January 2006
Available online 24 February 2006

Abstract

A new one-dimensional tellurite phosphate, $Ba_2TeO(PO_4)_2$ has been synthesized by standard solid-state reaction techniques using $BaCO_3$, TeO_2, and $(NH_4)H_2PO_4$ as reagents. The structure of $Ba_2TeO(PO_4)_2$ was determined by single-crystal X-ray diffraction. $Ba_2TeO(PO_4)_2$ crystallizes in the triclinic space group $P\text{-}1$ (No. 2), with $a = 6.9461(16)$ Å, $b = 7.3970(17)$ Å, $c = 8.887(2)$ Å, $\alpha = 76.843(4)^\circ$, $\beta = 79.933(4)^\circ$, $\gamma = 75.688(4)^\circ$, $V = 427.40(17)$ Å^3, and $Z = 2$. $Ba_2TeO(PO_4)_2$ has a novel one-dimensional chain structure that is composed of PO_4 tetrahedra and TeO_5 polyhedra. Te^{4+} cations are in asymmetric coordination environments attributable to their lone pairs. The lone pairs on the Te^{4+} cations point in the [100] and [−100] direction and interact with the Ba^{2+} cations. Infrared, Raman, and UV–Vis diffuse reflectance spectroscopy, thermogravimetric analysis, and dipole moment calculations are also presented.

Keywords: Synthesis; Tellurite; Phosphate; One-dimensional structure

1. Introduction

Mixed metal tellurites exhibit varying structural topologies owing to the nonbonded electron pair on the Te^{4+} cation [1–4]. Attributable to this lone pair, a local acentric coordination environment is also observed. In fact, lone pair cations such as Te^{4+}, not only exhibit asymmetric coordination environments, but these environments influence the material's properties [5–7]. The asymmetric coordination environment and lone pair are thought to be result of a second-order Jahn–Teller (SOJT) distortion [8–13]. A SOJT distortion reduces the energy between the highest occupied (HOMO) *s*-orbital and the lowest unoccupied (LUMO) *p*-orbital through *s–p* mixing [14–17]. The observed coordination numbers for Te^{4+} cations are three, four, and five, which result in various structural geometries such as distorted trigonal pyramidal, seesaw, and distorted square pyramidal, respectively [18,19]. Furthermore, when this distorted coordination geometry is combined with octahedral or tetrahedral moieties, a number of interesting framework architectures are possible. In addition with transition metal oxyphosphate compounds, a wide variety of structural topologies such as one-dimensional chains [1,20], two-dimensional layers [21–23], and three-dimensional frameworks [24–26] have been observed. Thus, combining these building blocks, Te^{4+} polyhedra and oxyphosphate groups, would result in interesting structural topologies. With these ideas in mind, we investigated materials in the Ba–Te–P-oxide system. With respect to tellurite phosphate oxides, a few materials have been reported, namely, $Te_2O_3(HPO_4)$ [27,28], $Te_8O_{10}(PO_4)_4$ [29], $A_2TeMo_2O_6(PO_4)_2$ (A = K, Rb, Cs, or Tl) [30], and $BaTeNbO_4(PO_4)$ [31]. Structurally the materials are different; $BaTeNbO_4(PO_4)$ contains two-dimensional layers; whereas, $Te_2O_3(HPO_4)$, $Te_8O_{10}(PO_4)_4$, and $A_2TeMo_2O_6(PO_4)_2$ exhibit three-dimensional structures consisting of asymmetric TeO_4 and TeO_5 polyhedra that are linked through oxygen atoms. In this paper, we report the synthesis, structure, and characterization of a uni-dimensional material, $Ba_2TeO(PO_4)_2$, representing a new quaternary tellurite phosphate with a novel crystal structure.

*Corresponding author. Fax: +1 713 743 0796.
E-mail address: psh@uh.edu (P. Shiv Halasyamani).

0022-4596/$ - see front matter © 2006 Elsevier Inc. All rights reserved.
doi:10.1016/j.jssc.2006.01.045

2. Experimental

2.1. Synthesis

$BaCO_3$ (Aldrich, 99 + %), TeO_2 (Aldrich, 99 + %), and $(NH_4)H_2PO_4$ (Aldrich, 98 + %) were used as received. Single-crystals of $Ba_2TeO(PO_4)_2$ were prepared by using excess amount of TeO_2 in order to promote crystal growth. 0.197 g (1.00 mmol) of $BaCO_3$, 0.115 g (1.00 mmol) of $(NH_4)H_2PO_4$, and 0.319 g (2.00 mmol) of TeO_2 were mixed with an agate mortar and pestle and introduced into a platinum crucible. The crucible was heated to 650 °C for 15 h and then cooled down to 500 °C at a rate of 6 °C h^{-1} before being quenched to room temperature. Colorless block-shaped crystals of $Ba_2TeO(PO_4)_2$ (42% yield based on tellurium) were recovered from the crucible with TeO_2. Pure polycrystalline $Ba_2TeO(PO_4)_2$ was synthesized through standard solid-state reaction. A stoichiometric mixture of $BaCO_3$ (1.316 g, 6.66 mmol) with TeO_2 (0.532 g, 3.33 mmol) and $(NH_4)H_2PO_4$ (0.767 g, 6.66 mmol) was thoroughly ground with an agate mortar and pestle and pressed into a pellet, which was introduced into an alumina crucible. The pellet was heated to 650 °C at a rate of 5 °C min^{-1}, held for 48 h, and cooled to room temperature (5 °C min^{-1}) with an intermediate regrinding. Powder X-ray diffraction (XRD) on the resultant white powder indicated a single-phase product, and was in a good agreement with the calculated pattern from the single-crystal structure (see supporting information).

2.2. Crystallographic determination

The structure of $Ba_2TeO(PO_4)_2$ was determined by standard crystallographic methods. A colorless block crystal ($0.10 \times 0.10 \times 0.12\,mm^3$) was used for single-crystal XRD. Room temperature intensity data were collected on a Siemens SMART diffractometer equipped with a 1 K CCD area detector using graphite monochromated Mo$K\alpha$ radiation. A hemisphere of data was collected using a narrow-frame method with scan widths of 0.30° in omega, and an exposure time of 30 s $frame^{-1}$. The first 50 frames were remeasured at the end of the data collection to monitor instrument and crystal stability. The maximum correction applied to the intensities was <1%. The data were integrated using the Siemens SAINT program [32], with the intensities corrected for Lorentz, polarization, air absorption, and absorption attributable to the variation in the path length through the detector faceplate. Ψ-scan was used for the absorption correction on the hemisphere of data. The data were solved and refined using SHELXS-97 and SHELXL-97, respectively [33,34]. All of the atoms were refined with anisotropic displacement parameters and converged for $I > 2\sigma(I)$. All calculations were performed using the WinGX-98 crystallographic software package [35]. Crystallographic data, atomic coordinates and displacement parameters, and selected bond distances and angles for $Ba_2TeO(PO_4)_2$ are given in Tables 1–3. The

Table 1
Crystal data for $Ba_2TeO(PO_4)_2$

Empirical formula	$Ba_2TeO(PO_4)_2$
Formula weight	608.22
Crystal system	Triclinic
Space group	*P*-1 (No. 2)
Z	2
a (Å)	6.9461(16)
b (Å)	7.3970(17)
c (Å)	8.887(2)
α (°)	76.843(4)
β (°)	79.933(4)
γ (°)	75.688(4)
Volume (Å^3)	427.40(17)
Temperature (K)	293.0(2)
ρ_{calc} (g cm^{-3})	4.726
μ (mm^{-1})	12.902
Crystal color	Colorless
Crystal habit	Block
Crystal size	$0.10 \times 0.10 \times 0.12$
Reflections collected	2611
Independent reflections	1834
R(int)	0.0261
T_{min}, T_{max}	0.225, 0.267
No. of parameters	128
Goodness-of-fit on F^2	1.212
X-ray radiation (λ, Å)	Mo$K\alpha$ (0.71073)
θ range (°)	2.37–27.98
Limiting indices	$-8 \leqslant h \leqslant 8$, $-9 \leqslant k \leqslant 9$, $-11 \leqslant l \leqslant 7$
Refinement method	Full-matrix least-squares on F^2 [SHELXL-97]
Final $R^{a,b}$ indices [$I > 2\sigma(I)$]	$R(F) = 0.0230$, $R_w(F_o^2) = 0.0624$
R indices (all data)	$R(F) = 0.0242$, $R_w(F_o^2) = 0.0629$
Largest diff. peak and hole (e Å^{-3})	0.848 and −0.809

[a] $R(F) = \Sigma||F_o|-|F_c||/\Sigma|F_o|$.
[b] $R_w(F_o^2) = [\Sigma w(F_o^2-F_c^2)^2/\Sigma w(F_o^2)^2]^{1/2}$.

Table 2
Atomic coordinates for $Ba_2TeO(PO_4)_2$

Atom	*x*	*y*	*z*	U_{eq}[a] (Å^2)
Ba(1)	0.3691(1)	0.8049(1)	0.4162(1)	0.013(1)
Ba(2)	0.1056(1)	0.3830(1)	0.2434(1)	0.013(1)
Te(1)	0.3525(1)	0.8881(1)	0.9547(1)	0.010(1)
P(1)	0.1351(2)	1.1218(2)	0.6483(2)	0.011(1)
P(2)	0.3755(2)	0.5215(2)	0.8164(2)	0.011(1)
O(1)	0.5512(6)	0.3504(6)	0.8568(5)	0.014(1)
O(2)	0.2726(6)	1.1107(6)	0.7801(5)	0.016(1)
O(3)	0.6200(6)	0.9284(6)	0.8986(5)	0.014(1)
O(4)	0.4647(6)	0.7041(6)	0.8018(5)	0.015(1)
O(5)	0. 1972(6)	0.5292(6)	0.9400(5)	0.015(1)
O(6)	0.3285(6)	0.5215(6)	0.6554(4)	0.015(1)
O(7)	0.0652(7)	0.9354(6)	0.6776(5)	0.020(1)
O(8)	0.2786(6)	1.1481(6)	0.4967(5)	0.016(1)
O(9)	−0.0395(6)	1.2917(6)	0.6520(5)	0.020(1)

[a] U_{eq} is defined as one third of the trace of the orthogonalized U_{ij} tensor.

X-ray powder diffraction data were collected on a Scintag XDS2000 diffractometer at room temperature (Cu$K\alpha$ radiation, $\theta-\theta$ mode, flat plate geometry) equipped with

Table 3
Selected bond distances (Å) and angles (°) for $Ba_2TeO(PO_4)_2$

Bond distances		Bond valence
Te(1)−O(1)	2.198(4)	0.5431
Te(1)−O(2)	2.028(4)	0.8294
Te(1)−O(3)	1.917(4)	1.0948
Te(1)−O(3)	2.144(4)	0.6197
Te(1)−O(4)	2.062(4)	0.7610
Bond valence sum of Te(1)		3.8480
P(1)−O(2)	1.612(4)	1.0183
P(1)−O(7)	1.526(4)	1.2417
P(1)−O(8)	1.534(4)	1.2184
P(1)−O(9)	1.517(4)	1.2656
Bond valence sum of P(1)		4.7440
P(2)−O(1)	1.550(4)	1.1742
P(2)−O(4)	1.591(4)	1.0696
P(2)−O(5)	1.504(4)	1.3048
P(2)−O(6)	1.522(4)	1.2531
Bond valence sum of P(2)		4.8017
Bond angles		
O(3)−Te(1)−O(2)	87.02(17)	
O(3)−Te(1)−O(4)	79.72(16)	
O(2)−Te(1)−O(4)	92.33(16)	
O(3)−Te(1)−O(3)	74.62(17)	
O(2)−Te(1)−O(3)	92.26(16)	
O(4)−Te(1)−O(3)	153.65(15)	
O(3)−Te(1)−O(1)	91.06(16)	
O(2)−Te(1)−O(1)	178.04(15)	
O(4)−Te(1)−O(1)	87.75(15)	
O(3)−Te(1)−O(1)	86.81(15)	

Peltier germanium solid-state detector in the 2θ range 5–60° with a step size of 0.02°, and a step time of 1 s.

2.3. Spectroscopic characterizations

Infrared data were recorded on a Matteson FTIR 5000 spectrometer in the 400–4000 cm^{-1} range, with the sample pressed between two KBr pellets. The Raman spectrum was recorded at room temperature on a Digilab FTS 7000 spectrometer equipped with a germanium detector with the powder sample placed in separate capillary tubes. Excitation was provided by a Nd:YAG laser at a wavelength of 1064 nm, and the output laser power was 544 mW. The spectral resolution was about 4 cm^{-1}, and 200 scans were collected. UV–Vis diffuse reflectance data for $Ba_2TeO(PO_4)_2$ were collected with a Varian Cary 500 scan UV–Vis–NIR spectrophotometer over the spectral range 200−1500 nm at room temperature. Polytetrafluoroethylene was used as a reference material. Reflectance spectrum was converted to absorbance with the Kubelka–Munk values [36].

2.4. Thermogravimetric analysis

Thermogravimetric analysis was performed on a TGA 2950 Thermogravimetric Analyzer (TA Instruments). The polycrystalline $Ba_2TeO(PO_4)_2$ sample was contained within a platinum crucible and heated at a rate of 10 °C min^{-1} from room temperature to 900 °C in static air.

3. Results and discussion

3.1. Structure

$Ba_2TeO(PO_4)_2$ is a new one-dimensional tellurite phosphate compound containing chains that run parallel to the *b*-axis. The chains are composed of PO_4 and TeO_5 units connected by P−O−Te and Te−O−Te bonds (see Fig. 1). As can be seen in Fig. 1, the two $[P(1)O_{1/2}O_{3/1}]^{2-}$ and $[P(2)O_{2/2}O_{2/1}]^{-}$ anionic tetrahedra and a $[TeO_{5/2}]^{-}$ polyhedron link to form one-dimensional chains. The two $[TeO_{5/2}]^{-}$ polyhedra share edges through O(3) and produce Te_2O_8 dimers (see Fig. 2). These dimers are further connected by the $[P(2)O_{2/2}O_{2/1}]^{-}$ anions through O(1) and O(4) to form a chain along [010] direction. An intrachain connection is made, between the $[P(1)O_{1/2}O_{3/1}]^{2-}$ and $[TeO_{5/2}]^{-}$ polyhedra through O(2) (see Fig. 1). The lone pairs on the Te^{4+} point in the [100] and [−100] direction which interact with the Ba^{2+} cations.

There are two crystallographically unique P^{5+} cations in the $Ba_2TeO(PO_4)_2$ structure. Both P^{5+} cations are in tetrahedral environments connected to four oxygen atoms. The P−O bond distances for each PO_4 tetrahedron range from 1.504(4) to 1.612(4) Å. The O−P−O bond angles range from 103.1(2) to 114.3(2)°. The Te^{4+} cation is in an asymmetric coordination environment attributable to its stereoactive lone pair. The Te^{4+} cation is in distorted square pyramidal environment bonded to five oxygen atoms resulting in TeO_5 polyhedra (see Fig. 2). The Te−O bond distances range from 1.917(4) to 2.198(4) Å. The O−Te−O bond angles range from 74.62(17) to 178.04(15)°. The two unique Ba^{2+} cations are in eight- and ten-fold coordination environments with Ba−O contacts ranging from 2.655(4) to 3.282(4) Å. In connectivity terms, $Ba_2TeO(PO_4)_2$ can be formulated as consisting of $\{[TeO_{5/2}]^{-}[P(1)O_{1/2}O_{3/1}]^{2-}\ [P(2)O_{2/2}O_{2/1}]^{-}\}^{4-}$ anionic chains, with charge balance maintained by the two Ba^{2+} cations. Bond valence calculations [37,38] resulted in values range 2.04−2.16, 4.74−4.80, and 3.85 for Ba^{2+}, P^{5+}, and Te^{4+}, respectively.

3.2. Infrared and Raman spectroscopy

The infrared and Raman spectra of $Ba_2TeO(PO_4)_2$ revealed Te−O, P−O, and Te−O−P vibrations. Te−O vibrations are observed in both the IR and Raman and found around 650−880 and 430 cm^{-1}. P−O vibrations are also observed in both the IR and Raman and occur at about 950−1150 and 450−570 cm^{-1}. A band, occurring around 600 cm^{-1}, is attributable to Te−O−P vibration. The infrared and Raman vibrations and assignments for $Ba_2TeO(PO_4)_2$ are listed in Table 4. The assignments are consistent with those previously reported [31,39,40].

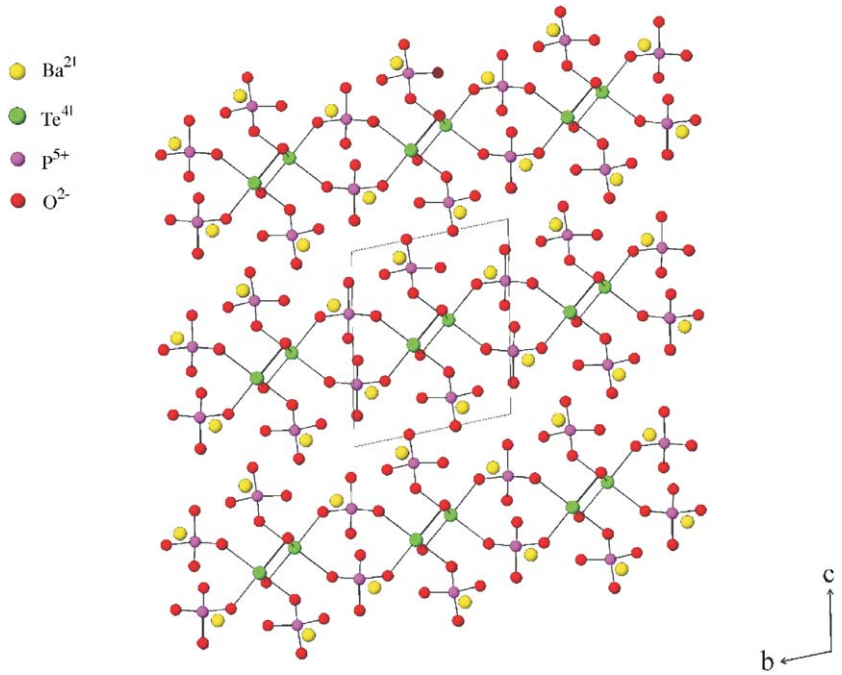

Fig. 1. Ball-and-stick diagram showing one-dimensional structure of $Ba_2TeO(PO_4)_2$ in the *bc*-plane. Note the chains run along the *b*-axis.

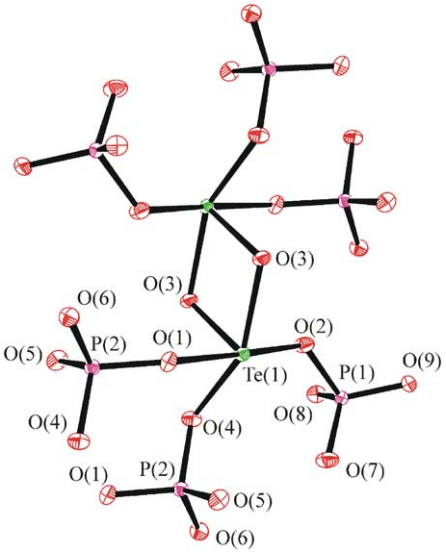

Fig. 2. ORTEP (50% probability ellipsoids) drawing for $Ba_2TeO(PO_4)_2$. The Ba^{2+} cations are removed for clarity. Note 4-coordinate tetrahedral and 5-coordinate distorted pyramidal environments for P^{5+} and Te^{4+} cations, respectively.

Table 4
Infrared and Raman vibrations for $Ba_2TeO(PO_4)_2$

P–O	Te–O	P–O–Te
IR (cm^{-1})		
1149	887	619
1103	831	603
1081	656	
1047	430	
983		
964		
576		
557		
538		
453		
Raman (cm^{-1})		
1161	860	613
1095	837	
1060	659	
972	432	
952		
574		
555		
536		
505		
459		

3.3. UV–Vis diffuse reflectance spectroscopy

$Ba_2TeO(PO_4)_2$ is white and the spectrum shows that it is transparent. Absorption (K/S) data were calculated from the following Kubelka–Munk function:

$$F(R) = \frac{(1-R)^2}{2R} = \frac{K}{S},$$

where R represents the reflectance, K the absorption, and S the scattering. In a K/S vs. E (eV) plot, extrapolating the linear part of the rising curve to zero provides the onset of absorption at 3.6 eV for $Ba_2TeO(PO_4)_2$. The overall band gap for the material may be attributable to the degree of the distortions arising from TeO_5 and PO_4 polyhedra. The

UV–Vis diffuse reflectance spectrum for $Ba_2TeO(PO_4)_2$ is deposited in the Supporting Information.

3.4. Thermogravimetric analysis

The thermal behavior of $Ba_2TeO(PO_4)_2$ was investigated using thermogravimetric analysis. $Ba_2TeO(PO_4)_2$ is not stable at high temperature. A single-step decomposition occurs at 730 °C attributable to the condensation of phosphate groups with simultaneous volatilization of TeO_2 at higher temperature. Powder XRD measurement on the calcined material revealed $Ba_2TeO(PO_4)_2$ decomposed to $Ba_2P_2O_7$ [41]. The decomposition is consistent with the following reaction:

$$Ba_2TeO(PO_4)_2 \xrightarrow[\Delta]{} Ba_2P_2O_7 + TeO_2.$$

The thermogravimetric analysis diagram for $Ba_2TeO(PO_4)_2$ and powder XRD pattern for calcined material, $Ba_2P_2O_7$ are deposited in the Supporting Information.

3.5. Dipole moment calculations

Although $Ba_2TeO(PO_4)_2$ crystallizes in centrosymmetric space group, the material contains a cation in an asymmetric coordination environment, i.e., Te^{4+}. One of our motivations for investigating materials containing asymmetric lone pair cations is to better understand these coordination environments. The direction and magnitude of the distortions in the TeO_5 polyhedra may be quantified by determining the local dipole moments. This approach has been described earlier [42–44]. The method uses a bond-valence approach to calculate the direction and magnitude of the local dipole moments. With the lone pair polyhedra, the lone pair is given a charge of −2 and the localized Te^{4+}-lone pair distance is estimated to be 1.25 Å [45]. Using this methodology, the dipole moment for the TeO_5 polyhedra is approximately 7.14 Debyes (D). In fact, an examination of 30 examples of TeO_5 polyhedra reveals that the dipole moments range from 4.31 to 10.82 D and average value of 8.33 ± 1.33 D (see Table 5). With $Bi_{10}Te_2O_{17}I_4$ [46], a relatively small dipole moment of 4.31 D is estimated, which may be attributable to the disorder between $Bi(3)^{3+}$ and $Te(1)^{4+}$ cations. The TeO_5 polyhedron contains shorter bond distances than BiO_5 group. In addition, Te^{4+} lone pair is more "directional" than that of Bi^{3+} based on the coordination environment. We are in the process of examining all Te^{4+} oxides that contain TeO_3, TeO_4, or TeO_5 groups in order to better understand the asymmetric polar environment [47].

Table 5
Calculation of dipole moments for TeO_5 polyhedra

Compound	TeO_5	Dipole moment (D)
$Ba_2TeO(PO_4)_2$[a]	$Te(1)O_5$	7.14
$BaTe_2O_6$ [48]	$Te(2)O_5$	7.75
$Bi_2Te_2O_8$ [49]	$Te(2)O_5$	7.19
$Ca(TeO)_2(TeO_6)$ [50]	$Te(1)O_5$	8.40
$Cs_2Te_4O_9$ [51]	$Te(2)O_5$	8.58
$In_2Te_3O_9$ [52]	$Te(2)O_5$	10.08
$K_2Te_4O_9$ [19]	$Te(1)O_5$	7.46
$K_2Te(Te_3O_{12})$ [53]	$Te(5)O_5$	8.41
$Na_2Te_4O_9$ [54]	$Te(1)O_5$	7.96
$NiTe_2O_5$ [55]	$Te(2)O_5$	7.79
$Te_2Se_2O_8$ [56]	$Te(1)O_5$	7.64
	$Te(2)O_5$	7.13
Te_3SeO_8 [57]	$Te(1)O_5$	8.64
$Te_8O_{10}(PO_4)_4$ [29]	$Te(1)O_5$	10.82
	$Te(2)O_5$	9.64
$TeSeO_4$ [58]	$Te(1)O_5$	7.89
$Tl_2Te_2O_5$ [59]	$Te(1)O_5$	8.90
$(Ag_{0.4}Na_{1.6})Te_5O_{14}$ [60]	$Te(3)O_5$	7.78
	$Te(4)O_5$	5.43
$Bi_4Te_2O_9Br_2$ [61]	$Te(2)O_5$	8.22
$Bi_{10}Te_2O_{17}I_4$ [46]	$Te(1)O_5$	4.31
$Ca_2Te_2O_4(CO_3)_2$ [62]	$Te(1)O_5$	7.71
$GdTe_2O_5Cl$ [63]	$Te(1)O_5$	9.74
$InTeO_3Cl$ [64]	$Te(1)O_5$	9.72
$Na_2MoTe_4O_{12}$ [65]	$Te(2)O_5$	7.89
$Na_2WTe_4O_{12}$ [65]	$Te(2)O_5$	7.73
$NaGaTe_2O_6$ [66]	$Te(1)O_5$	10.80
$NdTe_2O_5Br$ [67]	$Te(2)O_5$	10.23
$NdTe_2O_5Cl$ [63]	$Te(1)O_5$	9.02
$NH_4TeTeO_5(OH)$ [68]	$Te(1)O_5$	8.64
Average	TeO_5	8.33 (±1.33)

D = Debyes.
[a]This work.

4. Supporting information available

Powder XRD (calculated and experimental), UV–Vis diffuse reflectance spectrum, IR and Raman spectra, thermogravimetric analysis diagram for $Ba_2TeO(PO_4)_2$, and powder XRD pattern for calcined material, $Ba_2P_2O_7$ are available (PDF). Further details of the crystal structure investigation can be obtained from the Fachinformationszentrum Karlsruhe, 76344 Eggenstein-Leopoldshafen, Germany, (fax: (49) 7247-808-666; e-mail: crysdata@fiz.karlsruhe.de) on quoting the depository number CSD-416032.

Acknowledgments

We thank the Robert A. Welch Foundation for support. This work was also supported by the NSF-Career Program through DMR-0092054, and by the NSF-Chemical Bonding Center. P.S.H. is a Beckman Young Investigator. We also acknowledge Yushin Park and Prof. Rigoberto Advincula for assistance in obtaining the Raman spectra.

References

[1] M.F. Zid, T. Jouini, N. Jouini, C.R. Acad. Sci. Ser. IIc: Chim. 309 (1989) 343.

[2] Y. Arnaud, M.T. Averbuch-Pouchot, A. Durif, J. Guidot, Acta Crystallogr. B 32 (1976) 1417.
[3] J.A. Alonso, A. Castro, E. Gutierrez-Puebla, M.A. Monge, I. Rasines, C. Ruiz-Valero, J. Solid State Chem. 69 (1987) 36.
[4] V. Balraj, K. Vidyasagar, Inorg. Chem. 37 (1998) 4764.
[5] R. Seshadri, N.A. Hill, Chem. Mater. 13 (2001) 2892.
[6] U.V. Waghmare, N.A. Spaldin, H.C. Kandpal, R. Seshadri, Phys. Rev. B 67 (2003) 125111.
[7] P. Baettig, C.F. Schelle, R. LeSar, U.V. Waghmare, N.A. Spaldin, Chem. Mater. 17 (2005) 1376.
[8] U. Opik, M.H.L. Pryce, Proc. R. Soc. London A 238 (1957) 425.
[9] R.F.W. Bader, Mol. Phys. 3 (1960) 137.
[10] R.F.W. Bader, Can. J. Chem. 40 (1962) 1164.
[11] R.G. Pearson, J. Am. Chem. Soc. 91 (1969) 4947.
[12] R.G. Pearson, J. Mol. Struct. (THEOCHEM) 103 (1983) 25.
[13] R.A. Wheeler, M.-H. Whangbo, T. Hughbanks, R. Hoffmann, J.K. Burdett, T.A. Albright, J. Am. Chem. Soc. 108 (1986) 2222.
[14] H. Nikol, A. Vogler, J. Am. Chem. Soc. 113 (1991) 8988.
[15] H. Nikol, A. Vogler, Inorg. Chem. 32 (1993) 1072.
[16] G.W. Watson, S.C. Parker, J. Phys. Chem. B. 103 (1999) 1258.
[17] G.W. Watson, S.C. Parker, G. Kresse, Phys. Rev. B 59 (1999) 8481.
[18] M. Tatsumisago, T. Minami, Y. Kowada, H. Adachi, Phys. Chem. Glasses 35 (1994) 89.
[19] C.R. Becker, S.L. Tagg, J.C. Huffman, J.W. Zwanziger, Inorg. Chem. 36 (1997) 5559.
[20] M.M. Borel, A. Leclaire, J. Chardon, C. Michel, J. Provost, B. Raveau, J. Solid State Chem. 135 (1998) 302.
[21] M. Fakhfakh, M.F. Zid, N. Jouini, M. Tournoux, J. Solid State Chem. 102 (1993) 368.
[22] T. Hoareau, A. Leclaire, M.M. Borel, A. Grandin, B. Raveau, J. Solid State Chem. 116 (1995) 87.
[23] M.M. Borel, A. Leclaire, J. Chardon, J. Provost, B. Raveau, J. Solid State Chem. 137 (1998) 214.
[24] M. Fakhfakh, A. Verbaere, N. Jouini, Eur. J. Solid State Inorg. Chem. 29 (1992) 563.
[25] M. Fakhfakh, S. Ammar-Merah, N. Jouini, Solid State Sci. 2 (2000) 587.
[26] A. Leclaire, J. Chardon, J. Provost, B. Raveau, J. Solid State Chem. 163 (2002) 308.
[27] H. Mayer, Z. Kristallogr. 141 (1975) 354.
[28] N.W. Alcock, W.D. Harrison, Acta Crystallogr. B 38 (1982) 1809.
[29] H. Mayer, G. Pupp, Z. Kristallogr. 145 (1977) 321.
[30] A. Guesdon, B. Raveau, Chem. Mater. 12 (2000) 2239.
[31] K.M. Ok, J. Orzechowski, P.S. Halasyamani, Inorg. Chem. 43 (2004) 964.
[32] SAINT, Version 4.05, Siemens Analytical X-ray Systems, Inc., Madison, WI, 1995.
[33] G.M. Sheldrick, SHELXS-97—A Program for Automatic Solution of Crystal Structures, University of Goettingen, Goettingen, Germany, 1997.
[34] G.M. Sheldrick, SHELXL-97—A Program for Crystal Structure Refinement, University of Goettingen, Goettingen, 1997.
[35] L.J. Farrugia, J. Appl. Crystallogr. 32 (1999) 837.
[36] P. Kubelka, F. Munk, Z. Tech. Phys. 12 (1931) 593.
[37] I.D. Brown, D. Altermatt, Acta Crystallogr. B 41 (1985) 244.
[38] N.E. Brese, M. O'Keeffe, Acta Crystallogr. B 47 (1991) 192.
[39] A.A. Belik, F. Izumi, M. Azuma, T. Kamiyama, K. Oikawa, K.V. Pokholok, B.I. Lazoryak, M. Takano, Chem. Mater. 17 (2005) 5455.
[40] P.E. Tomaszewski, M. Maczka, A. Majchrowski, A. Waskowska, J. Hanuza, Solid State Sci. 7 (2005) 1201.
[41] A.A. El Beghitti, A. Elmarzouki, A. Boukhari, E.M. Holt, Acta Crystallogr. C 51 (1995) 1478.
[42] P.A. Maggard, T.S. Nault, C.L. Stern, K.R. Poeppelmeier, J. Solid State Chem. 175 (2003) 25.
[43] H.K. Izumi, J.E. Kirsch, C.L. Stern, K.R. Poeppelmeier, Inorg. Chem. 44 (2005) 884.
[44] K.M. Ok, P.S. Halasyamani, Inorg. Chem. 44 (2005) 3919.
[45] J. Galy, G. Meunier, J. Solid State Chem. 13 (1975) 142.
[46] P.S. Berdonosov, D.O. Charkin, A.M. Kusainova, C.H. Hervoches, V.A. Dolgikh, P. Lightfoot, Solid State Sci. 2 (2000) 553.
[47] K.M. Ok, P.S. Halasyamani, in preparation.
[48] M. Kocak, C. Platte, M. Troemel, Acta Crystallogr. B 35 (1979) 1439.
[49] P. Thomas, B. Jeansannetas, J.C. Champarnaud-Mesjard, B. Frit, Eur. J. Solid State Inorg. Chem. 33 (1996) 637.
[50] H. Effenberger, J. Zemann, H. Mayer, Am. Miner. 63 (1978) 847.
[51] B.O. Loopstra, K. Goubitz, Acta Crystallogr. C 42 (1986) 520.
[52] E. Philippot, R. Astier, W. Loeksmanto, M. Maurin, J. Moret, Rev. Chim. Miner. 15 (1978) 283.
[53] F. Daniel, J. Moret, M. Maurin, E. Philippot, Acta Crystallogr. B 34 (1978) 1782.
[54] S.L. Tagg, J.C. Huffman, J.W. Zwanziger, Chem. Mater. 6 (1994) 1884.
[55] C. Platte, M. Troemel, Acta Crystallogr. B 37 (1981) 1276.
[56] C. Delage, A. Carpy, M. Goursolle, C.R. Acad. Sci. C Chim. 295 (1982) 981.
[57] C. Pico, A. Castro, M.L. Veiga, E. Gutierrez-Puebla, M.A. Monge, C. Ruiz-Valero, J. Solid State Chem. 63 (1986) 172.
[58] Y. Porter, N.S.P. Bhuvanesh, P.S. Halasyamani, Inorg. Chem. 40 (2001) 1172.
[59] B. Jeansannetas, P. Thomas, J.C. Champarnaud-Mesjard, B. Frit, Mater. Res. Bull. 33 (1998) 1709.
[60] W. Loeksmanto, J. Moret, M. Maurin, E. Philippot, J. Solid State Chem. 33 (1980) 209.
[61] L.N. Kholodkovskaya, V.A. Dolgikh, B.A. Popovkin, J. Solid State Chem. 116 (1995) 406.
[62] R. Fischer, F. Pertlik, J. Zemann, Can. Miner. 13 (1975) 383.
[63] G.B. Nikiforov, A.M. Kusainova, P.S. Berdonosov, V.A. Dolgikh, P. Lightfoot, J. Solid State Chem. 146 (1999) 473.
[64] E. Gaudin, J.-P. Chaminade, A. El Abed, J. Darriet, Acta Crystallogr. C 57 (2001) 1004.
[65] V. Balraj, K. Vidyasagar, Inorg. Chem. 38 (1999) 5809.
[66] R. Miletich, F. Pertlik, J. Alloys Compd. 268 (1998) 107.
[67] I.V. Tarasov, V.A. Dolgikh, L.G. Aksel'rud, P.S. Berdonosov, B.A. Ponovkin, Zh. Neorg. Khim. 41 (1996) 1243.
[68] E. Philippot, L. Benmiloud, M. Maurin, J. Moret, Acta Crystallogr. B 35 (1979) 1986.